Eur. Phys. J. A **30**, 591–601 (2006)
DOI 10.1140/epja/i2006-10144-3

THE EUROPEAN PHYSICAL JOURNAL A

Multifoil UC_x target for the SPES project —An update

A. Andrighetto[1], C.M. Antonucci[2], S. Cevolani[2], C. Petrovich[2,a], and M. Santana Leitner[3]

[1] INFN Laboratori Nazionali di Legnaro, Viale dell'Università 2, 35020 Legnaro (PD), Italy
[2] ENEA, Via M.M. Sole 4, 40129 Bologna, Italy
[3] AB-Department, CERN, 1211 Geneve 23, Switzerland

Received: 20 June 2006 / Revised: 18 October 2006 /
Published online: 5 December 2006 –
Communicated by C. Signorini

Abstract. The target system is one of the key issues for the facilities aimed at the production of neutron-rich radioactive ion beams. In the framework of the SPES project (Study for the Production of Exotic Species), the possibility of using a target configuration with a proton beam (40 MeV, 0.2 mA) directly impinging on multiple uranium carbide disks is investigated. The ^{238}U fission fragments constitute the source for the exotic beams and for this purpose the disks are placed inside a graphite box at 2000 °C. The target is split into several thin disks in order to allow the cooling of the system by thermal radiation. In this way about $\sim 10^{13}$ fissions s^{-1} are obtained with a relative simple system and with relative low costs. Further steps have been performed compared to previous publications and now all the main parameters of the system have been analysed by means of calculation codes: the fission rates and the fission fragment distribution; the power deposition and the thermal analysis; the thermo-mechanical behaviours of the disks; the effusive and diffusive extraction release properties of the target.

PACS. 29.25.Rm Sources of radioactive nuclei – 24.10.Lx Monte Carlo simulations (including hadron and parton cascades and string breaking models) – 25.85.Ge Charged-particle-induced fission

1 Introduction

Intense neutron-rich isotope beams open many new fields of investigation, such as nuclear-structure studies in a yet unexplored region. Several laboratories are trying to produce high enough intensities to warrant a new generation of experiments. The present study is inserted in the framework of the R&D of the SPES project (Study for the Production of Exotic Species) [1–3], an accelerator based facility for the production of intense neutron-rich radioactive ion beams, in the range of masses between 80 and 160. SPES is a new-generation ISOL facility proposed in Italy at the INFN-LNL (Istituto Nazionale di Fisica Nucleare, Laboratori Nazionali di Legnaro), able to represent a competitive intermediate step between the existing facilities and the longer-range high-performance facility EURISOL [4]. Between EURISOL and SPES there will be two orders of magnitude in beam power in the direct target, in the production of specific isotopes and likely in financial investment. The nominal fission rate is $10^{15}\,s^{-1}$ for EURISOL and $10^{13}\,s^{-1}$ for SPES, both using a ^{238}U target, under uranium carbide form.

A possible target configuration for the radioactive ion beam projects is the 2-step solution, consisting of a proton (or deuteron) beam impinging on a converter target used to emit fast neutrons for fissioning the uranium target. On the other hand, the 1-step solution is chosen here, consisting of a 40 MeV proton beam (0.2 mA) directly impinging on the fission target, composed by uranium carbide. The target is split into several thin disks in order to allow the cooling of the system (by thermal radiation) by increasing the total exchange surface. The advantage of this configuration is its simplicity in the cooling system and the consequent relatively low cost.

The configuration has already been proposed in a previous paper [3]: the proton beam enters from the window, then it slows down and induces fissions within the disks and finally it is absorbed by some dump structure. In this way it is possible to drive in the UC_x disks only the protons with higher fission cross-section (those with higher energy). The disks are inserted inside a cylindrical box which, for reasons concerning the extraction of the fission fragments produced in the disks, has to be held at 2000 °C. This target structure is in turn inserted inside an external chamber. From a thermal point of view, such a chamber is the actual heat well of the whole system: the disks will in fact radiate (thermally) towards the box which, in turn, radiates towards the external chamber walls.

[a] e-mail: carlo.petrovich@bologna.enea.it

The analysis of the target presented in [3] mainly concerned the study of the beam-target interaction and the target thermal analysis. The main purposes were to show the good performances of such a system in terms of fission fragment production and of coolability. After having reached these objectives, some further steps have been performed:

- an improvement of the target layout [5], by using a higher number of disks (in this way the fission events per incident proton are increased and the average power per disk is lowered), a dump structure also in form of disks (the design is simplified also by avoiding the necessity of an exit window), a box made of graphite instead of tungsten (a better heat transfer is allowed and chemical reactions between the tungsten and the uranium carbide are avoided);
- a more comprehensive analysis including also the detail beam profile;
- the verification of the mechanical stability of the disks;
- the estimate of the diffusion/effusion times.

Firstly, the target reference layout will be presented in detail (sect. 2). Then the main characteristics of the system are analyzed by means of computer codes: the fission rates and the fission fragment distribution (sect. 3) for the estimation of the source of the system (the radioactive beams); the distribution of the power deposition (sect. 3) that has been used for the detailed thermal analysis (sect. 4). The results of the thermal study are in turn used as input for the thermo-mechanical analysis (sect. 5). Finally, the effusion and the diffusion issues, concerning the time spent from the production of atoms until their extraction from the system, are faced in the last section (sect. 6).

Up to now, no assessment has been performed concerning either the window mechanical stability or the possible losses of fission atoms through the graphite walls of the box and the window (see sect. 2). It is to be said, however, that our candidate material, which is pyrolytic graphite, has virtually no porosity and the losses should be negligible.

2 Target configuration

In this section the target reference configuration will be described. Before doing this, some results concerning a 40 MeV proton beam impinging on a UC_x thick target are discussed. These results are obtained from a simulation by means of the MCNPX 2.5.0 code [6] and have the purpose of understanding better the physics of the system and the choice of some parameters for the target configuration.

2.1 Thick target calculations

A 40 MeV proton beam impinging on a UC_x thick target (the isotopic ratio of the depleted uranium compared to the carbon is assumed to be U : C = 1 : 4) of density 2.5 g/cm^3 has a range of $\sim$ 1.2 cm. With MCNPX it is possible to predict the maximum fission rate available for this proton beam energy and, at the same time, to analyze how the fission rates and the power deposition would change for target thicknesses lower than the proton range. With 0.2 mA, the total fission rate in the thick target turns out to be $9.1 \cdot 10^{12}$ fissions s^{-1} and the total power deposition about 8.2 kW (8 kW is the power of the 0.2 mA, 40 MeV beam; then the Q-values of all the reactions, including fissions, are considered). The accumulation along the target depth of the fission rates and of the power deposition up to these two values ($9.1 \cdot 10^{12}$ s^{-1} and 8.2 kW) is shown in fig. 1. This allows to estimate the total UC_x disk thickness that would minimize the power deposition in the disks without loosing too many fission events. From fig. 1 it can be deduced that a total UC_x thickness of about 9 mm is a good compromise: 92% of the total possible fission events are obtained, while about 57% of the power is deposited.

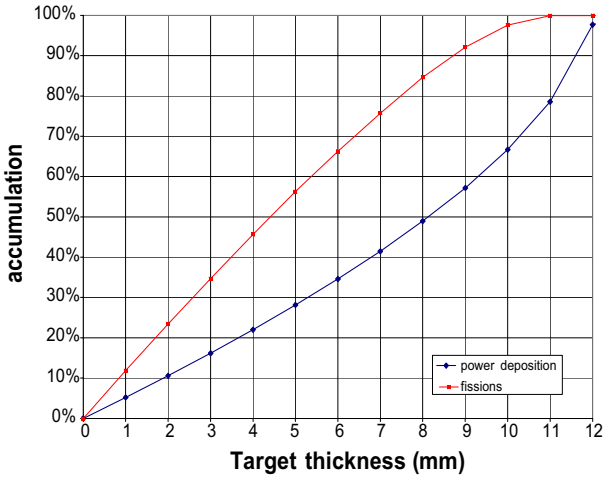

Fig. 1. Accumulation of the fission rates and of the power deposition by a 40 MeV proton beam on a thick UC_x target.

2.2 Target description

The target is split into seven UC_x disks, which integrate a total UC_x thickness of 9.3 mm (see fig. 2). For the sake of thermal behaviour, the thicknesses of the disks have been set in order to distribute the power as uniformly as possible in the disks. In this way the power deposition in each disk is lowered. Thus, the beam traverses progressively thinner disks, as a compensation mechanism to the

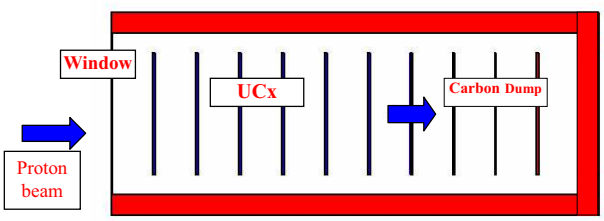

Fig. 2. Reference target configuration.

increasing values of the stopping energy per length of the protons.

In the choice of the beam profile, thermal considerations were also instrumental: a uniform distribution of the beam has been chosen in order to flatten as much as possible the power deposition inside the disks.

The detailed parameters used for the following analysis are:

- the 40 MeV proton beam has a current of 0.2 mA. The beam profile spans uniformly over a circle distribution of radius = 3 cm, which matches the disk radii;
- the window (necessary to separate the beam line from the target void regions) is constituted by a thin carbon foil of 400 μm;
- the UC_x target (2.5 g/cm^3) is made up of 7 disks with thicknesses from 1.4 mm down to 1.2 mm (66 g of total mass);
- the beam dump is composed of 3 carbon disks with thicknesses varying from 0.8 mm up to 1 mm. Here the lower-energy protons having lower production rate and higher stopping power are driven;
- the box containing the disks is made of graphite.

3 Power deposition and isotope production

In this section some fundamental results for the target, such as the fission rate, the fission fragment distribution and the power deposition, are shown. These have been calculated by means of the Monte Carlo radiation transport code MCNPX 2.5.0 [6]. This code, together with some considerations about its accuracy, is introduced in the next section.

3.1 Some considerations on the MCNPX code

The MCNPX code allows a detailed 3D definition of the system to be analyzed and a full transport calculation, starting from the proton particle distribution. For the description of the nuclear interactions, MCNPX usually uses evaluated cross-section libraries. When these are missing (like for protons interacting with ^{238}U), MCNPX offers different physics models describing the nuclear interactions by the transition of different stages: Intra-Nuclear Cascade, pre-equilibrium stage, evaporation/fissions, de-excitation. The models chosen here are the Bertini-Dresner model [7] together with the ORNL (Oak Ridge National Laboratory) [8] model for the fission fragment distribution. A validation of the fission cross-sections predicted by the Bertini model in the range 10–40 MeV has been already performed in [3] providing discrepancies in the range 10%–30%. On the other hand, the accuracy for the fission fragment distribution is lower and, unfortunately, the production of specific nuclei concerns precisely the final goal of the SPES project. A comparison of the ORNL fission model and the RAL [9] (Rutherford Appleton Laboratory) fission model with experimental data is reported in [10], but only for incident protons > 100 MeV.

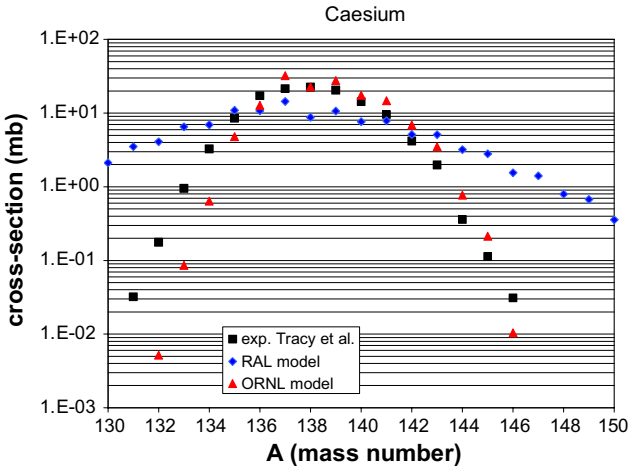

Fig. 3. Comparison between MCNPX and experimental data for caesium [11].

Moreover, only the overall mass distribution is considered there, without analyses of the isotope distributions.

Some comparisons between the MCNPX calculations and the experimental data provided by [11] have been here performed for a 40 MeV proton impinging on a thin ^{238}U target. The results for caesium, obtained by using the ORNL fission model and the RAL fission model, are shown in fig. 3. The RAL model (default option for MCNPX) does not work properly except at the peaks. The general distribution is well described by the ORNL model, even if some data have discrepancies of more than one order of magnitude.

3.2 Results

The following results are obtained through MCNPX calculations performed for the target configuration described previously. It turns out that a power of 0.19 kW is deposited in the window, 4.1 kW in the seven UC_x disks, 1.7 kW into the three dump disks and 2.2 kW is lost outside the disks (some protons scatter and are deflected outwards). Thus, the average power deposition for the UC_x target disks is about 4.1 kW/7 disks = 0.58 kW. The power deposition with its radial profile in all the disks is reported in table 1 and shown in fig. 4. As expected, the radial profile is uniform in the window (following the entering uniform beam profile) and it becomes less and less flattened in the last disks, because of the proton scattering. The highest ratio between the maximum power density and the average power density in the UC_x disks turns out to be max /avg = 1.4.

The calculated fission rate in all the 7 disks approached $7.6 \cdot 10^{12}$ fissions s^{-1} ($1.5 \cdot 10^{13}$ atoms s^{-1} are thus produced). The peak-to-valley ratio in the mass number distribution of the fission products, that is very pronounced in thermal neutron-induced fissions at about $A = 115$–120, is here only of about a factor of 2. The experimental data reported in [12] for 35 MeV protons on ^{238}U show very similar factors. This was an intended result since the ra-

Table 1. Power deposition in all the disks (the disks have radius = 3 cm).

	Thickness	Power deposition	$0 < r < 0.3$ cm	$0.3 < r < 0.6$ cm	$0.6 < r < 0.9$ cm	$0.9 < r < 1.2$ cm	$1.2 < r < 1.5$ cm	$1.5 < r < 1.8$ cm	$1.8 < r < 2.1$ cm	$2.1 < r < 2.4$ cm	$2.4 < r < 2.7$ cm	$2.7 < r < 3.0$ cm
	mm	Watt	W/cm^3	W/cm^3	W/cm^3	W/cm^3	W/cm^3	W/cm^3	W/cm^3	W/cm^3	W/cm^3	W/cm^3
C window	0.4	189	168	167	167	167	167	167	167	167	167	167
Disk n. 1	1.4	583	148	148	148	148	148	148	148	148	148	144
Disk n. 2	1.4	595	156	155	155	155	155	155	155	155	155	130
Disk n. 3	1.4	606	165	164	164	164	164	164	164	163	157	113
Disk n. 4	1.3	570	175	175	176	175	175	175	173	167	147	102
Disk n. 5	1.3	580	190	189	189	190	189	186	179	164	138	99
Disk n. 6	1.3	589	208	207	207	204	200	192	179	159	133	98
Disk n. 7	1.2	560	230	228	224	218	210	196	179	158	133	101
Dump n. 1	0.8	539	343	339	331	319	302	280	255	225	191	151
Dump n. 2	0.7	583	417	414	401	386	365	340	311	278	241	199
Dump n. 3	1	595	301	296	288	276	261	242	221	197	172	143

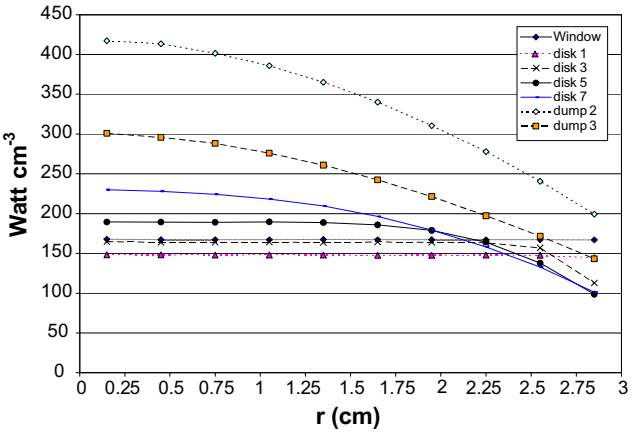

Fig. 4. Radial distribution of the power deposition in the disks.

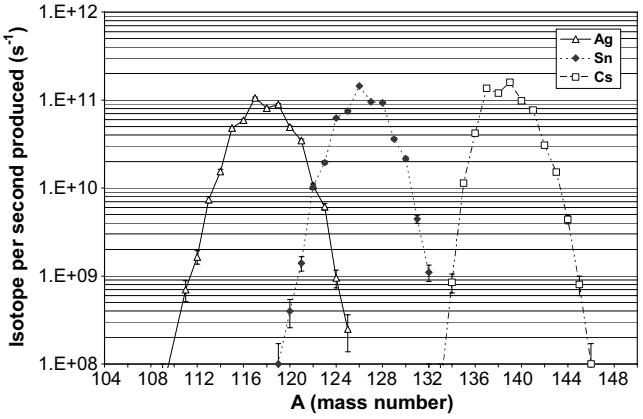

Fig. 5. Mass distribution for silver, tin and caesium.

dioactive ion beams should lie precisely in the mass range $80 < A < 160$.

The isotope production for some interesting atoms (Ag, Sn, Cs) is shown in fig. 5, reaching values up to $\sim 10^{11}$ atoms/s. The ^{132}Sn isotope, being a double-magic nucleus, is one of the radioactive nuclei of interest. Its production is here estimated to be $\sim 10^9\,\mathrm{s}^{-1}$. Even if the predictive accuracy of these data is quite limited, the ratio between the production of ^{126}Sn (the peak) and the production of ^{132}Sn, is very close to the one predicted in [13] with a different theoretical model [14] (a factor ~ 120 is there estimated for 50 MeV protons on ^{238}U).

These results reveal promising features for the proposed target configuration. A first crucial check point in the validation of the system feasibility is the thermal status of the disks and of the carbon box.

4 Thermal behaviour

As mentioned before, the box has to be kept at 2000 °C so as to enhance the fission product extraction. In order to ensure this condition, the target thermal analysis will be subdivided into two steps.

In the first one, called *disk thermal analysis*, the heat transfer between the disks and the box is studied. The main input data is the power deposition in each disk (table 1 and fig. 4) and the heat is transmitted towards the box by thermal radiation only. In the frame of this analysis, the box is assumed to be at the required temperature, 2000 °C; such a temperature is also considered to be uniform all over the box. The analysis will be extended both to the target and to the dump disks.

In the second step, called *box thermal analysis*, the thermal equilibrium of the box is examined. The box is again assumed to be at uniform temperature, subjected

Table 2. Physical properties of the materials of interest.

Property	Uranium carbide	Source	Graphite	Source
Melting point [°C]	2390 °C	[15]	> 3600	[17]
	2450 °C	[16]		
	2527 °C	[18]		
Thermal conductivity [$W\,m^{-1}\,C^{-1}$]	1.0	[19]	100	[17]
Emissivity [-]	0.60	[19]	0.80	[17]

to a double power deposition (the heat coming from the disks and the direct effect of the beam scattering) and thermally radiating towards a chamber at about room temperature. As already verified for the previous target layout [3], the total heat deposited in the box will not be sufficient for holding it at the requested temperature (2000 °C); as a consequence, the result of this analysis will be the amount of power to be added to the box by means of an independent heat source (for the possibility to use thermal shields, see sect. 4.2).

Both steps are performed in steady-state conditions. To what refers the physical properties of the materials constituting the target (uranium carbide and graphite), the literature data shown in the table 2 were used. As resulting from that table, the target disk material melting point is characterized by a relative high spreading; in the following, the lowest value will be taken as reference.

4.1 Disk thermal analysis

The temperature field in the disks was evaluated by means of the computer code MOD3, a model already used for the evaluations presented in [5] and described in that paper. This steady-state code represents an improvement of the models discussed in [20] and is mainly devoted to the analysis of conduction and radiation heat transfer in disk systems; for the determination of the view factors among annular meshes, the algebraic method presented in [21] was adopted. Parallel analyses were also performed by means of the ANSYS code, whose results (see, for example, fig. 6) are in good agreement with the MOD3 ones.

As input data for the MOD3 calculations, the power deposited in each disk and the power deposition profiles are those shown in table 1 and fig. 4. Due to the fact that the circumferential power deposition is assumed to be uniform, 2D calculations were performed; in radial direction 15 meshes were used, while just 7 were apparently sufficient in the thickness/axial (beam) direction.

A summary of the input data and of the obtained results is shown in table 3 for both target and dump disks. The temperatures given here are the maximum computed temperatures for each disk, *i.e.* the temperature at the disk midplane; and the maximum temperature differences

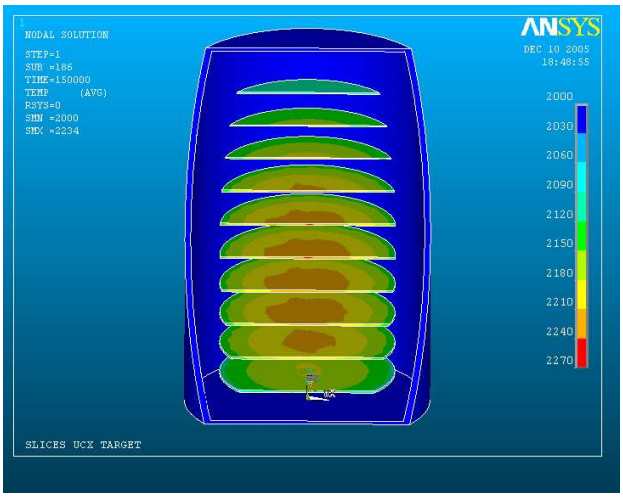

Fig. 6. Temperature ANSYS calculation.

Table 3. Disk analysis: summary of input data and results.

Disk	Thickness [mm]	Power [W]	T_{max} [°C]	ΔT_{max} in radial direction [°C]	ΔT_{max} in thickness direction [°C]
Window	0.4	189	2069	22	≈ 0
Target 1	1.4	583	2167	31	36
Target 2	1.4	595	2175	50	38
Target 3	1.4	606	2180	68	41
Target 4	1.3	570	2176	78	39
Target 5	1.3	580	2186	88	40
Target 6	1.3	589	2195	98	44
Target 7	1.2	560	2194	101	41
Dump 1	0.8	539	2136	68	3
Dump 2	0.7	583	2142	68	3
Dump 3	1.0	595	2145	70	4

both in radial and in thickness direction; these are important features for the thermo-mechanical analysis of sect. 5.

Looking at the maximum temperatures of the target disks, it appears that they are sensibly below the minimum literature value of the melting point (see table 2). The maximum temperature is found in the disks n. 6 and n. 7, both about at the same temperature; such disks are the hottest not due to the power, about the same in all the disks, but due to the power profile, becoming more peaked in the last disks (see fig. 4).

For the same reason, also the thermal gradients increase in the beam direction. The most important one is the gradient in the radial direction, always sensibly greater than the one along the thickness. With respect to the gradients, the maximum is to be found in the disk n. 7, but very close to the one of disk n. 6.

In order to perform the thermo-mechanical analysis, a full matrix of the temperatures in radial and thickness direction of the disk n. 6 was used. Such matrix is visualized

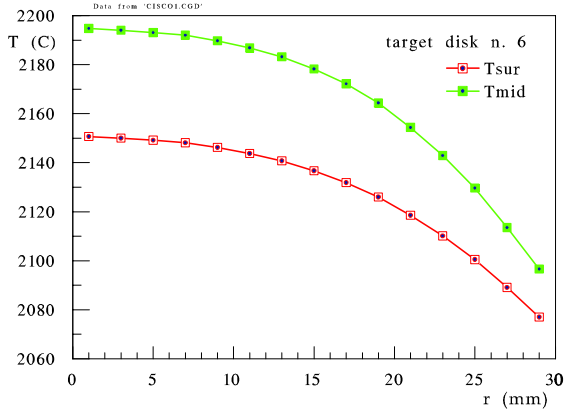

Fig. 7. Disk n. 6 temperature profile in the radial direction.

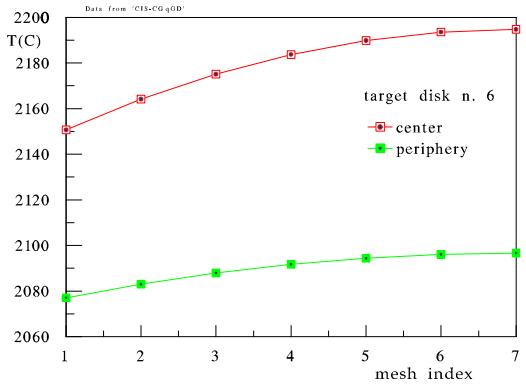

Fig. 8. Disk n. 6 temperature profile in the thickness direction.

in figs. 7 and 8. The first one shows the radial temperature profile at the disk surface and on the disk midplane. In fig. 8 two temperature profiles in the thickness direction are given: the first one at the disk centre and the other one at the disk periphery.

From the computed average surface temperature of the disks (about 2100 °C) it becomes possible to evaluate the average vapour pressure of the uranium carbide. This is inferred from the data presented in [22]. The obtained value (about $1 \cdot 10^{-2}$ Pa) is in agreement with the limiting criteria proposed in the same paper.

Finally, in view of further developments of the target design, the possibility (from a thermal point of view) to reduce the target disks radius was examined. Such analysis was performed by means of parametric MOD3 calculations, concerned not only with the disk diameter but also with the disk number, thickness and spacing [5]; anyway, the total power was taken constant, *i.e.* in first approximation without changing the target performances. The calculations are very preliminary, especially because the present power profiles were used for many different configurations. The results show that it would be possible to reduce the disk radius down to about 60% of the present ones without reaching the melting point. If the results of recent analyses on the uranium carbide material [23] are confirmed, then the thermal emissivity of this material is greater than that assumed in the present calculation, allowing for a further reduction of the disk diameter or for an increase of the margin to melting.

Table 4. Box shielding: summary of input data and results.

	Box	Shield n. 1	Shield n. 2	Chamber
Diameter [mm]	80	110	140	–
Length [mm]	220	220	220	–
Emissivity [-]	0.80	0.25	0.25	0.25
Temperature [°C]	2000	1782	1289	50

4.2 Graphite box thermal analysis

The graphite box is heated by the beam scattered particles and by the thermal radiation from the disks: the total amount of deposited heat was evaluated from table 1 and reaches 8145 W. At the same time, the box is cooled by the thermal radiation towards some external chamber held at about room temperature, here assumed to be 50 °C.

This situation cannot be reached if the box surface has to be held at 2000 °C: if we impose such temperatures, the heat transferred from the box to the chamber walls turns out to be $Q = 70.5$ kW.

This is about ten times the heat actually supplied to the box. As a consequence, in order to hold the graphite box at the requested temperature it becomes necessary to heat the box (independently from the power due to the beam) by about 62 kW.

This independent box heating is a desired feature: it allows for a better control of the target system and for the safety of the start-up and shut-down procedures. However, it would be better if the required power could be lowered. For this reason, the possibility to insert some tungsten thermal shields between the graphite box and the chamber was examined. Such an analysis was tentatively evaluated by means of a simple *ad hoc* model. By applying it to the actual target and imposing a total heat transfer of 8145 W, the results shown in table 4 were obtained.

It appears that a couple of shields of thickness equal to 1 mm each would suffice to eliminate the need for box heating. It has to be pointed out that this analysis was not performed in order to find out a shield layout able to avoid the box heating but only to demonstrate the possibility to drive (reduce) the amount of heat to be supplied to the box by means of shields.

5 Thermo-mechanical analysis

In accordance with the temperature distribution given by the previously described thermal analysis, a calculation has been carried out of the thermo-mechanical state of stress developed in disk n. 6, whose values of gradient and temperature are intended to be representative of the most conservative operating condition. The calculation, however, is drastically simplified by the assumptions made of

elastic material and steady-state regime; moreover, the results are difficult to interpret because the physical properties of UC_x are substantially unknown when the temperature approaches the melting point. Research on this point should be pursued and would be recommendable to perform mechanical property measurements on a real batch of candidate material rather than to only rely on available data.

5.1 Physical properties of uranium carbide

At this point it was necessary to get hold of specific technical literature, particularly [24] which is a rather comprehensive survey.

A value suggested [24,25] for the elastic modulus of UC is $E = 215\,\text{GPa}$ at room temperature and it is proposed together with a matching value for the Poisson's ratio $\mu = 0.269$. The temperature dependence of the modulus is quite pronounced and shows obviously a negative slope. A curve for the decrease in E for UC between room temperature and 1500 °C is proposed in [24] and has been employed for extrapolating to a reference temperature $T_{\text{ref}} = 2000\,^{\circ}\text{C}$; the corresponding value is $E = 176\,\text{GPa}$, but the extrapolation from 1500 °C to 2000 °C is arbitrary. No corrections have been applied to the elastic modulus for the effect of porosity, nor to the Poisson's ratio for the effect of both temperature and porosity.

Two values [24] suggested for the mean thermal linear expansion coefficient of UC refer to temperature 1000 °C and 2000 °C. Thus the value adopted $\alpha_{\text{m}} = 12.4 \cdot 10^{-6}\,^{\circ}\text{C}^{-1}$ at 2000 °C does not need extrapolation. Once again, no correction for porosity has been applied.

As to fracture behaviour, UC is a brittle ceramic material which may be susceptible to catastrophic fracture at low temperature, but a brittle-ductile transition is expected to occur at some temperature in the range 1100–1300 °C. This does not imply that the material deforms completely plastically above ∼ 1300 °C, although, at least to a certain extent, plasticity should assure its role in the relaxation of thermal stress. Values of fracture stress are given up to ∼1300 °C only, where [24] it becomes $\sigma \cong 200\,\text{MPa}$.

The conclusion is that the assumption of linearity seems rather adequate up to ∼ 1300 °C, but it seems more questionable beyond, and therefore the study has been iterated at two different temperatures, respectively, of 1300 °C and 2000 °C. The first result (1300 °C) is fairly representative of the brittle behaviour when heating up from room temperature[1], while the second result (2000 °C) would set itself for now only as a sort of "best indicator" of the behaviour at the nominal point of operation. Further analyses and measurements would be needed for definitive results.

[1] With thermal shields, without box heating.

5.2 Modelling and results

As the UC disk absorbs the proton beam power, temperature gradients are generated across the material both in radial and axial directions. The state of stress resulting from such a non-uniform temperature distribution may cause different effects leading ultimately to fracture of the disk. We limited our examination to the effect of the differential thermal expansion originated by the non-uniform stationary temperature distribution.

Different approaches have been attempted and lead to very similar results.

Following an order-of-magnitude analysis [5] it is easy to calculate that the estimated stress should assume the approximate values of $\bar{\sigma} = 75\,\text{MPa}$ at 1300 °C and $\bar{\sigma} = 130\,\text{MPa}$ at 2000 °C.

A second class of solutions has been obtained through numerical treatment of the equations of linear elasticity both in one-dimensional and two-dimensional approaches [26,27].

In the one-dimensional approach the equations are approximated under plane stress assumption and the numerical treatment consents to deal with arbitrary radial temperature distribution and temperature dependence of material properties. Obviously, there can be no variation of physical parameters through the thickness of the disk, and the axial gradient of temperature must be neglected or somehow integrated into the radial gradient.

Results are given in form of Von Mises equivalent stress σ_{eq}, which is calculated through the combination of any number of principal components the state of stress is characterized by, and is comparable to a state of monoaxial stress.

The maximum value of the stress state is calculated at the edge of the disk, which is in tension, and where the tangential stress, $\sigma_\theta = 76\,\text{MPa}$ at 1300 °C and $\sigma_\theta = 116\,\text{MPa}$ at 2000 °C, is equal to the value σ_{eq} of the equivalent stress.

In the two-dimensional approach the effect of the non-uniform temperature distribution is taken into consideration both in radial and axial direction. A third component σ_z of the state of stress is added to the equations and the problem becomes a special case of three-dimensional elasticity (because of the axial symmetry of geometry and temperature).

The maximum tensile stress is located again at the edge of the disk and the tangential stress is now $\sigma_\theta = 100\,\text{MPa}$ at 2000 °C, to be compared with the previous value 116 MPa.

But the maximum equivalent stress is now located toward the center of the disk and its value is $\sigma_{\text{eq}} = 60\,\text{MPa}$ at 1300 °C and 138 MPa at 2000 °C.

The last step has been to model the geometry and physical properties of the disk using a commercially available code. ANSYS, a multi-purpose finite element package, was used for this task.

An axisymmetrical model of the disk has been developed by rotation of a rectangular area corresponding to 1/2 cross-section view. The element used has been a PLANE42 type, *i.e.* a basic 2D solid element supporting

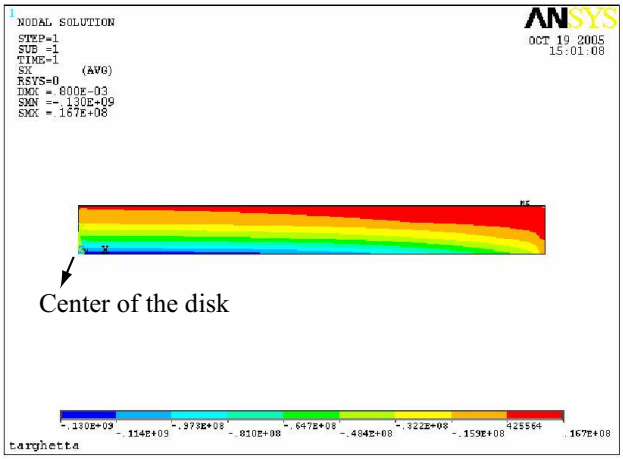

Fig. 9. Radial stress (Pa).

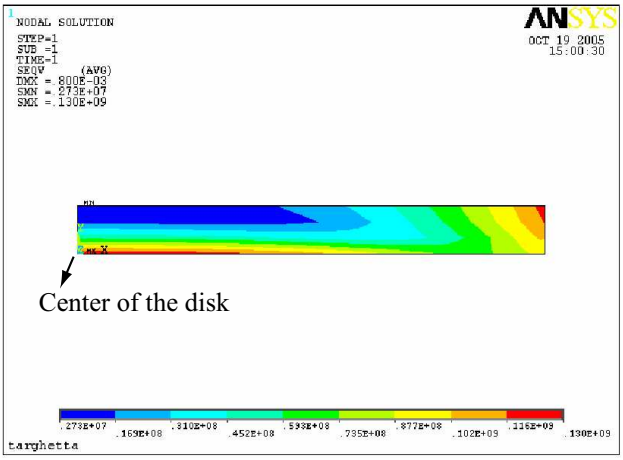

Fig. 11. Equivalent stress (Pa).

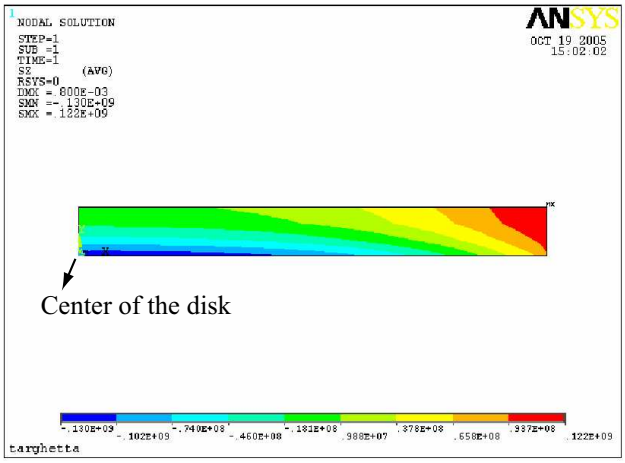

Fig. 10. Tangential stress (Pa).

axisymmetry. Material properties have been chosen to be comparable with those of the previous calculations.

The model has been loaded with the temperature distribution issued by the previously described thermal analysis. The temperature field in the original thermal calculation was distributed over 15×7 points located on a transversal section along the radius (1/4 of the total cross-section). Preprocessing has increased the original number, through linear interpolation, from 105 to 564 points corresponding to the total number of nodes used in the investigation. The representation of the node is a square with length of side ~ 0.2 mm.

The state of stress at 2000 °C is represented by the isochromics of radial stress σ_{r}, tangential stress σ_θ, and equivalent stress σ_{eq} reported in figs. 9, 10 and 11.

The maximum tensile stress is located again at the edge of the disk and its value is $\sigma_\theta = 122$ MPa to be compared with the values 116 MPa (one-dimensional model) and 100 MPa (two-dimensional model).

The value of the maximum equivalent stress is $\sigma_{\mathrm{eq}} = 130$ MPa at 2000 °C to be compared with 138 MPa (two-dimensional model).

It seems, therefore, that the equivalent stress, when the operating temperature keeps below the ductile-to-brittle transition temperature of the material (1300 °C), is inferior to the fracture strength at relevant temperature. This circumstance, on one hand, may render us confident about the risk of fracture due to differential expansion during the heating-up of the disk.

On the other hand, at temperatures below this transition, the disk may be much more susceptible to thermal shock and crack propagation; these modes of failure have not been analyzed hitherto.

Fatigue failure has not been analysed yet.

And, to end with brittle behaviour, a safe behaviour during the heating-up does not prevent risk of failure during the cooling-down.

At nominal temperature (2000 °C) the equivalent stress is low ($\sim$ 140 MPa), but the assumption of linearity is haphazard and the rheological properties of UC are unknown, however. Nevertheless, it should exhibit considerable plasticity and the elastic modulus should be very low. Therefore the stresses imposed on the disk should be probably negligible.

6 Isotope extraction analysis

The study of a target usually begins by surveying the expected generation of radioisotopes and examining whether the structure will withstand the energy deposited by the primary beam. These stages have been conducted in the previous sections by well-established nuclear transport codes and thermo-mechanical packages. The last step, covered here, is to investigate aspects related to the extraction of isotopes in order to assess about the outgoing intensity of the radioactive beam. Indeed, the stream of radioisotopes suffers a number of losses between the generation

phase in the target and the beam interaction in the experimental stations downstream the ion source. The most relevant of these are the intrinsic release efficiency, or loss of particles due to decay during slow diffusion (inside the solids) and effusion (free flight among target grains and foils), the ionization efficiency, and the target transmission efficiency (that accounts for the chemical absorptions of atoms in the walls of the system).

The previous entities tend to be antagonist and usually conflict with the rules dictated for appropriate isotope generation and good thermal behaviour. As an example, some facilities aim at boosting the RIB intensities by using large targets filled with dense powders because of the big amount of produced isotopes and the favourable heat conductivity. However, in some of those cases, the characteristic diffusion times, which scale to the second power of the thickness of the solid, and the effusion paths (*i.e.*, number of absorptions) may become excessively high and could widely cancel out all the positive factors. Similar contradicting arguments are found between the diffusive and the effusive release, and between the intrinsic release efficiency and the ionization efficiency. The complex interrelations among the production and release phenomena justified the creation of a Monte Carlo code that would integrate them all. The program that fulfils this condition, called RIBO, has been used in series with MCNPX and ANSYS for the conceptual design of the SPES multifoil target, and is briefly introduced in the coming section (sect. 6.1).

6.1 The Radioactive Ion Beam Optimiser (RIBO) code

RIBO [28] is a Monte Carlo simulation program that tracks the paths of point-like objects (namely atoms or photons) moving within solid (still or moving) boundaries. The driving force for the project has been the creation of a tool that could predict the release of radioactive nuclei from ISOL targets. Thus, the code integrates the main phenomena involved in isotope extraction and ion beam formation: diffusion, effusion, ionization and ion transport, although in the present stage of the SPES study only the two first phenomena were considered.

In the validation of the SPES geometry through RIBO, the first step for the calculations was to define the *source of radioisotopes*. The code offers several standard sources as well as a routine to customize them, which was used to match the radioisotope generation to the distribution obtained with MCNPX (sect. 3).

The next step was to compute the *diffusion* of radioisotopes from the grains of UC_x in the powder. The Monte Carlo code includes a dedicated module to compute this process in powder, fiber or foils accounting for complex phenomena, *e.g.* space/time varying conditions, pulsed sources or diffusion-desorption coupling. This fan of options shall be useful to refine the calculations once the target is better characterized. For the time being, however, this module was not explicitly used, and the standard diffusion delays provided were used.

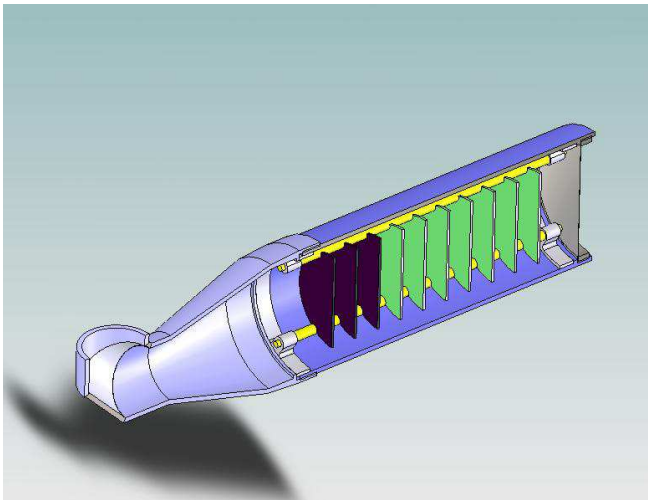

Fig. 12. Target layout.

The third step was the computation of the *effusive-diffusive* release of the isotopes through the powder grains in the UC pills. This process was computed by a module in the Monte Carlo code, which performs a random walk where the average distance (FP) between two atom-grain collisions is determined by the user in view of the density of the powder. The process stops when the atom exits the pill, but it will resume if the atom is reflected back into the UC_x volume. In particular, this means that atoms can traverse the pills in their exodus to the transfer line.

Sequentially, vacuum *effusion* constitutes the last step for the SPES preliminary simulations. This thermal energy transport process depends strongly on the atom-surface collision law. Among the various implemented models, the most suitable combination is the Lambert reflection and Maxwell-Boltzmann energy sampling, which are the default options in the Monte Carlo code. Moreover, effusion was simulated for an ideal molecular regime, that is to say, switching off the particle-particle interactions, available in RIBO for slightly pressurized systems. In order to emulate effusion through the system, an input file based in 3D combinatorial geometry had to be written to describe the SPES multifoil configuration. The code offers powerful tracking patterns, with intermediate milestone passage conditions and multiple path options, but in the concerned case, atoms were simply traced from generation up to a surface detector at the exit of the target conical aperture (see fig. 12).

The information generated in the output file, containing data of individual histories and a statistical analysis up to the 5th momentum was used to speculate about the release times for various reasonable diffusion and desorption values.

6.2 Modelling and results

The reference isotope was $A = 12$ (the choice is justified for compatibility with previous simulations, and anyway the results can be rescaled to other masses as mentioned

later in this section), and two sets of simulations were run, one for $FP = 15$ micron and another for $FP = 50$ micron, in order to observe the effect of the density of the powder in the release efficiency. In addition, a parallel simulation with identical parameters was run for the geometry of an ISOLDE-like UC target (IS), in view of comparing the efficiency of the SPES target with this world-known reference.

The first occurring process, *diffusion*, is very sensitive to the stoichiometry of the UC and to the grain size distribution. For the time being, the powder of ISOLDE and SPES will be considered equal, so no *relative* difference will be recorded for this concept. The experimental data collected at ISOLDE were instrumental to define an approximate *absolute* scale for diffusive release. Indeed, by comparing RIBO simulations and measured curves at ISOLDE, the diffusion time constants of various isotopes in UC matrices were coarsely estimated [28]. It was observed that the noble gases would diffuse slower than many other species, and that light elements diffuse better than heavier elements of similar chemical properties. For example, the computed diffusion time constant in UC_x powder was about 234 ms for ^{6}He, 2080 ms for ^{23}Ne, 8700 ms for ^{90}Kr and 1000 ms for ^{119}Sn. These numbers anticipate that diffusion will generally dominate the global release, although the fast fraction of released isotopes will be partially controlled by the effusion peak.

The results for the *effusion* from the SPES target suggest that the total flight path (150 m) is mostly (99%) performed outside the pills, and that the tightness of those has a limited impact ($\sim 0.01 \cdot FP$ [micron]%) on this number. However, $\sim$ 90–98% of the collisions take place within the powder pills (COLL), this number nearly scaling inversely to FP ($\sim 1.5 \cdot 10^6/FP$ [micron]). The number of collisions with the rest of the walls remains below 3000. The average effusive release time for the reference isotope ($A = 12$) results from adding the average flight time and the total adsorption-desorption time spent in the surfaces (below the time spent in surfaces other than the grains is neglected):

$$\begin{aligned} t_{\mathrm{e}}\,[\mathrm{ms}] &= 90 + \mathrm{COLL} \cdot t_{\mathrm{s}}\,[\mathrm{ms}] \\ &= 90 + 1.5 \cdot 10^6 \cdot t_{\mathrm{s}}\,[\mathrm{ms}]/FP\ [\mathrm{micron}], \end{aligned}$$

where the mean sticking time per collision (t_{s}) is a function of the chemical affinity between the isotope and the surface. For noble gases t_{s} is below 10^{-5} ms/collision, so that $t_{\mathrm{e}} \sim 90$ ms. It should be pointed out that the results for the flight time (90 ms) can be extrapolated to other isotopes by rescaling the obtained value to the square root of the isotope mass. For instance, the neutron-rich ^{95}Kr (with a half-life of 780 ms) would take $t_{\mathrm{e}} = 250$ ms to be extracted after diffusion.

As for the simulation with the reference IS geometry, it is confirmed that the free flight path (28 m) is shorter than that in SPES (148 m), the free volume of the first being much smaller. In exchange, the path through the powder in the IS target (70 m) is well above the number obtained for SPES (1.5 m) because the amount of UC in the latter is much lower. This fact has an impact also in the number of collisions, 50 times higher in the IS target. In conclusion, except for very inert species (*i.e.* noble gases), the release from the SPES target shall be significantly faster than that from the IS targets.

The preliminary results, in view of the ISOLDE numbers, and within reasonable values for the unknown parameters, give the impression that the SPES multifoil target can perform very efficiently for light and intermediate isotopes even with relatively high (microsecond) surface sticking times. The SPES target study includes a sensitivity analysis on the sticking time and diffusion time constant so that a global diffusion + effusion release fraction can be estimated based on the full release profile (and not only on the mean numbers) for any isotope of known diffusion coefficient and chemical affinity in the UC matrix.

Conclusions

A possible target configuration for the production of exotic nuclei has been analysed. With a proton beam of 40 MeV and 0.2 mA the fission rate turns out to be about $8 \cdot 10^{12}$ fissions s^{-1} (thus $1.6 \cdot 10^{13}$ atoms s^{-1} are produced).

The thermal analysis of the proposed layout shows the good coolability of the target and of the dump disks. The containing box has to be independently heated for holding it at the requested 2000 °C temperature; the necessary power has been evaluated. Anyway, by using suitable thermal shields the amount of heat to be supplied to the box can be reduced *ad libitum*.

In the framework of a preliminary analysis, the thermo-mechanical behaviour of a single disk of target has been examined under the assumption of steady-state operation and elastic behaviour of the uranium carbide. The second assumption in particular is a very rough approximation and needs further refinement. An order of magnitude has been estimated, followed by analyses carried out under different assumptions. We expected, as an order of magnitude, to compute stresses not beyond the range 130–280 MPa. Actually, the worst value of the equivalent stress that we calculated in accordance with our different assumptions is 140 MPa. This is to be compared to an (assumed) value for the rupture stress of 200 MPa.

To complete the study, the release from the SPES multifoil target and the ISOLDE UC target has been carefully compared by means of the RIBO thermal energy particle transport code. The simulations show that SPES target presents a good isotope extraction behaviour up to intermediate masses, remarkably faster than ISOLDE target for microsecond isotope-surface affinities. On the other side, due to their poor diffusion coefficients and the relatively long flight path in the SPES target, heavy short-lived noble gases will be extracted at lower rates.

We wish to thank G. Fortuna, F. Gramegna, J. Lettry, A. Pisent, and G. Prete for their precious collaboration and helpful discussions.

References

1. A. Bracco, A. Pisent (Editors), *SPES Technical Design for an Advanced Exotic Ion Beam Facility at LNL*, (REP)181/02 (LNL-INFN, 2002).
2. A. Andrighetto, J. Li, C. Petrovich, Q. You, Nucl. Instrum. Methods B **204**, 205 (2003).
3. A. Andrighetto, S. Cevolani, C. Petrovich, Eur. Phys. J. A **25**, 41 (2005).
4. J. Cornell (Editor), *The EURISOL Report – A feasibility study for a EURopean Isotope-Separation-On-Line radioactive ion beam facility* (GANIL, 2003) `http://www.ganil.fr/eurisol/`.
5. A. Andrighetto, C.M. Antonucci, S. Cevolani, C. Petrovich, *ENEA contribution to the design of the thin target for the SPES project*, FIS-P815-020 (ENEA, 2006) `http://www.bologna.enea.it/pubblicazioni.html`.
6. Denise B. Pelowitz (Editor), *MCNPX^{TM} User's manual*, Version 2.5.0, LA-CP-05-0369 (2005).
7. H.W. Bertini, Phys. Rev. **131**, 1801 (1963).
8. J. Barish, T.A. Gabriel, F.S. Alsmiller, R.G. Alsmiller jr., *HETFIS High-Energy Nucleon-Meson Transport Code with Fission*, ORNL-TM-7882 report (Oak Ridge National Laboratory, 1981).
9. F. Atchison, *Spallation and Fission in Heavy Metal Nuclei under Medium Energy Proton Bombardment*, in *Targets for Neutron Beam Spallation Sources*, Jul-Conf-34, Kernforschungsanlage Julich GmbH (1980).
10. T.W. Armstrong, P. Cloth, D. Filges, R.D. Neef, Nucl. Instrum. Methods Phys. Res. **222**, 540 (1984).
11. B.L. Tracy *et al.*, Phys. Rev. C **5**, 222 (1972).
12. V.A. Rubchenya *et al.*, Nucl. Instrum. Methods Phys. Res. A **463**, 653 (2001).
13. J. Äystö, V. Rubchenya, Eur. Phys. J. A **13**, 109 (2002).
14. M. Huhta *et al.*, Phys. Lett. B **405**, 230 (1997).
15. M.G. Saint-Laurent *et al.*, *Spiral Phase-II Final Report* (2001) `http://www.ganil.fr/research/sp/reports/files/Spiral_Phase2.pdf`.
16. L.C. Carraz *et al.*, Nucl. Instrum. Methods **158**, 69 (1979).
17. R.C. Weast (Editor), *Handbook of Chemistry and Physics* (CRC Press, 1974).
18. S. McLain, J.H. Martens (Editors), *Reactor Handbook* (Interscience Publishers, 1964).
19. J.A. Nolen, M. Petra, J. Greene, *Thermal Conductivity Measurements of Porous Materials at High Temperatures*, Physics Division Annual Report 1999, edited by K.J. Thayer (ANL, 2000).
20. S. Cevolani, *Valutazioni termiche su un Multifoil Target per TRADE*, FIS-P99R-003 (ENEA, 2004).
21. S. Cevolani, *Modelli per la determinazione dei fattori di vista fra mesh anulari di dischi coassiali paralleli*, FIS-P815-012 (ENEA, 2005).
22. G.D. Alton, J.R. Beene, Y. Liu, Nucl. Instrum. Methods Phys. Res. A **438**, 190 (1999).
23. J.P. Greene, A. Levand, J. Nolen, T. Burtseva, Nucl. Phys. A **746**, 425c (2004).
24. Hj. Matzke, *Science of Advanced LMFBR Fuels* (North Holland, 1980).
25. Balankin *et al.*, Atomn. Energ. **48**, 49 (1980).
26. Timoshenko, Goodier, *Theory of Elasticity* (McGraw Hill, 1970).
27. Z. Zudans, T.C. Yen, W.H. Steigelmann, *Thermal Stress Techniques in the Nuclear Industry* (Elsevier, 1965).
28. M. Santana Leitner, *A Monte Carlo Code to Optimize the Production of Radioactive Ion Beams by the ISOL Technique*, CERN-Thesis-2005-049, UPC-ETSEIB (Barcelona, 2005) p. 311.